Electrochemical Reduction of N_2 under Ambient Conditions for Artificial N_2 Fixation and Renewable Energy Storage Using N_2/NH_3 Cycle

Di Bao, Qi Zhang, Fan-Lu Meng, Hai-Xia Zhong, Miao-Miao Shi, Yu Zhang, Jun-Min Yan, Qing Jiang, and Xin-Bo Zhang*

Ammonia (NH_3) is one of the most highly produced chemicals because it is a source of nitrogen for fertilizer, a clean energy carrier, and a potential transportation fuel (due to its high energy density and lack of CO_2 emissions).[1–5] The total worldwide NH_3 production was 146 million tons in 2015,[6] and as human populations increase around the world, it is estimated that between one-third and one-half of the population will starve to death if ammonia-based fertilizers are not available in the future.[7] Although the availability of nitrogen (N_2) from the atmosphere for fixed N_2 production is unlimited, due to the stability and chemical inertness of N_2 (bond energy: 940.95 kJ mol^{-1}), it is a significant challenge to fix N_2 at ambient temperature and pressure.[8] Currently, the energy- and capital-intensive Haber–Bosch process (350–550 °C and 150–350 atm) still dominates NH_3 synthesis via a dissociative reaction that involves the coactivation of dihydrogen (H_2) and N_2, wherein the H_2 is mainly produced by steam reforming the natural gas (which produces large amounts of CO_2) and the energy required (>600 kJ mol^{-1} NH_3) is largely derived from fossil fuels.[9,10] Additionally, due to the unfavorable chemical equilibrium, ammonia yield is very low (conversion ratio: 10%–15%), and the process favors the formation of N_2 and H_2, even using such harsh conditions.[11]

Dr. D. Bao, F.-L. Meng, M.-M. Shi, Prof. J.-M. Yan, Prof. Q. Jiang
Key Laboratory of Automobile Materials (Jilin University)
Ministry of Education
Department of Materials Science and Engineering
Jilin University
Changchun 130022, China
E-mail: junminyan@jlu.edu.cn
Dr. D. Bao, Q. Zhang, F.-L. Meng, H.-X. Zhong, M.-M. Shi, Prof. X.-B. Zhang
State Key Laboratory of Rare Earth Resource Utilization
Changchun Institute of Applied Chemistry
Chinese Academy of Sciences
Changchun 130022, China
H.-X. Zhong
University of Chinese Academy of Sciences
Beijing 100049, China
Prof. Y. Zhang
Key Laboratory of Bio-Inspired Smart Interfacial Science and Technology of Ministry of Education
School of Chemistry and Environment
Beihang University
Beijing 100191, China

DOI: 10.1002/adma.201604799

Accordingly, significant efforts have been devoted to the artificial synthesis of ammonia by using biological (nitrogenase powered by adenosine triphosphate molecules), lightning, photocatalytic, and electrocatalytic methods (Figure S1, Tables S1 and S2, Supporting Information). However, these processes still have drawbacks, including relatively high temperatures (increased product decomposition), complex and expensive electrolytes, and difficulty in the regeneration of the active nitrogen-fixing complex, and/or low yields at ambient conditions. Theoretically, the thermodynamics of N_2 and NH_3 suggest that the electrochemical reduction of N_2 gas should proceed at negative potentials similar to those required by the H_2 evolution reaction. Additionally, electrochemical reduction is favored because it can be powered by a renewable electricity source, proceeds at moderate temperature, and atmospheric pressure.[12–15] Unfortunately, until now, no heterogeneous electrocatalysts have been discovered that can produce ammonia in significant yields at ambient conditions.

Previous theoretical studies have shown that stepped facets are the favorable active sites on catalysts and these facets optimize the activity of the metal-based catalysts.[5,16,17] The calculation results show that the intermediates in the N_2-fixing reaction are bound more strongly to the active sites located at steps than they are on flat terraces,[18] which improves the N_2 catalytic performance. We observed that tetrahexahedral (THH) Au is a typical noble metal enclosed by {730} crystal planes.[19,20] Due to its multifaceted surfaces composed of a mixture of various types of high-index sites, THH Au might achieve superior performance for N_2 adsorption and reduction.

Herein, as a proof-of-concept experiment, we propose and demonstrate that the electrocatalytic N_2 reduction reaction (NRR) is indeed possible at room temperature and atmospheric pressure by using tetrahexahedral gold nanorods [THH Au NRs, enclosed by stepped {730} facet, composed of (210) and (310) sub-facets] as a heterogeneous electrocatalyst. Unexpectedly, the THH Au NRs endowed the electrocatalytic NRR with a high production yield (NH_3: 1.648 μg h^{-1} cm^{-2}, N_2H_4 H_2O: 0.102 μg h^{-1} cm^{-2}) and low activation energy (≈13.704 kJ mol^{-1}) at –0.2 V (vs reversible hydrogen electrode (RHE)) under room temperature and atmospheric pressure, which is even comparable with the yield of N_2 fixation under high temperature and pressures, as listed in Table S1 (Supporting Information). Furthermore, a detailed reaction mechanism for the electrocatalytic NRR is outlined by density functional theory (DFT), and an alternate pathway is proposed.

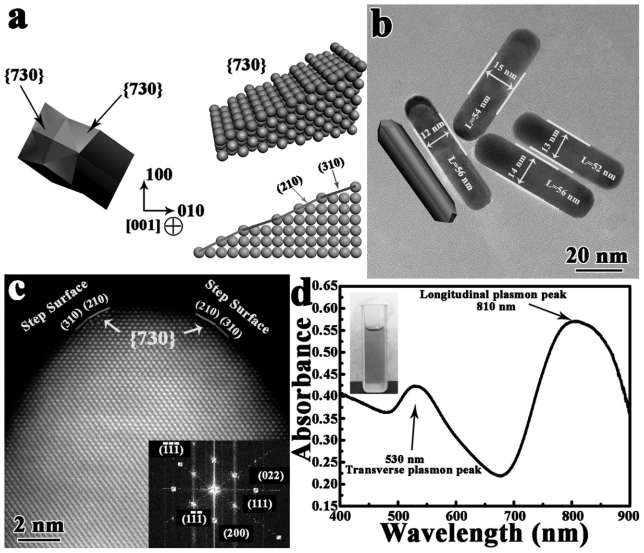

Figure 1. Atomic level surface structures of Au THH NR. a) Geometric models of an Au THH NR and exposed 24{730} facet. The {730} facet is composed of (210) and (310) sub-facets on Au NRs; b) TEM image of Au THH NRs with diameter: 12–15 nm, length: 52–56 nm, and aspect ratio: 4 ± 0.5; c) Spherical aberration corrected transmission electron microscope image of the Au THH NR with stepped sub-facets, the inset in (c) is the fast Fourier transform pattern of the indicated region; d) UV–vis extinction spectrum of the Au NRs, the inset is the photograph of as-obtained Au THH NRs suspended in water.

Before structural characterization and NRR tests, the THH Au NRs were washed and centrifuged (3000 rpm, 15 min) several times. The results of energy dispersive X-ray spectrometry indicate that the surfactant is washed off without any impurity, as shown in Figure S2 (Supporting Information). The morphological characterization, obtained via transmission electron microscopy (TEM), reveals the morphology of the THH Au NRs. Although the Au NRs typically exhibit cylindrical morphologies with two rounded ends, they are capped with square pyramids in the experimental tests, which are enclosed by multifaceted surfaces, as simulated in **Figure 1**a,b and Figure S3 (Supporting Information). The angles between the bases and bevels on a single THH Au NR were then measured, starting clockwise from the one labeled (Figure S4, Supporting Information). The measured angle indicates that the bevels on the THH Au NR are high-index {730} planes, which are charted by a calculated angle of ≈24°.[19] The atomic arrangements on the THH Au {730} facets are measured by spherical aberration corrected transmission electron microscope, the high resolution transmission electron microscopy (HRTEM) image is shown in Figure 1c, and the {730} is a multistep facet that is composed of the (210) and (310) sub-facets (Figure 1a). The ultraviolet–visible spectrum (UV–vis) of the obtained THH Au NRs is shown in Figure 1d. As shown, two peaks are present at 852 and 521 nm, which are likely due to the longitudinal plasmon and transverse plasmon, respectively. The blue shifts of the longitudinal plasmon and transverse peaks, compared to the published results,[21] suggest a decrease in the size of the products, which increases the number of exposed chemically active facets. Although catalytically active sites are abundant on the THH Au NRs, which can cap with the gas molecule, it remains challenging to correlate the catalytic activities with the atomic-level surface structures due to their intrinsic structural complexity. To further determine the electrocatalytic reduction ability and corresponding reaction pathway of the THH Au NRs, electrocatalytic NRR tests were conducted as followed.

N_2 gas is supplied in a feed gas stream to the cathode, where N_2 and water (H_2O) combine with electrons to form hydroxide (OH^-) and the N_2 reduction product. The electrolyte is a KOH solution (0.1 M), and the anodic reaction is the evolution of N_2, as described in **Figure 2**a. Based on the results calculated using the Nernst equation, the standard potential for the reduction of N_2 to NH_3 is 0.098 V vs RHE (Ag/AgCl/saturated KCl reference electrode has been calibrated on reversible hydrogen electrode, as shown in Figure S5, Supporting Information), which is calculated assuming that P_{N2} = 0.99 atm, P_{NH3} = 0.01 atm, and [KOH] = 0.1 M.[22] In this study,

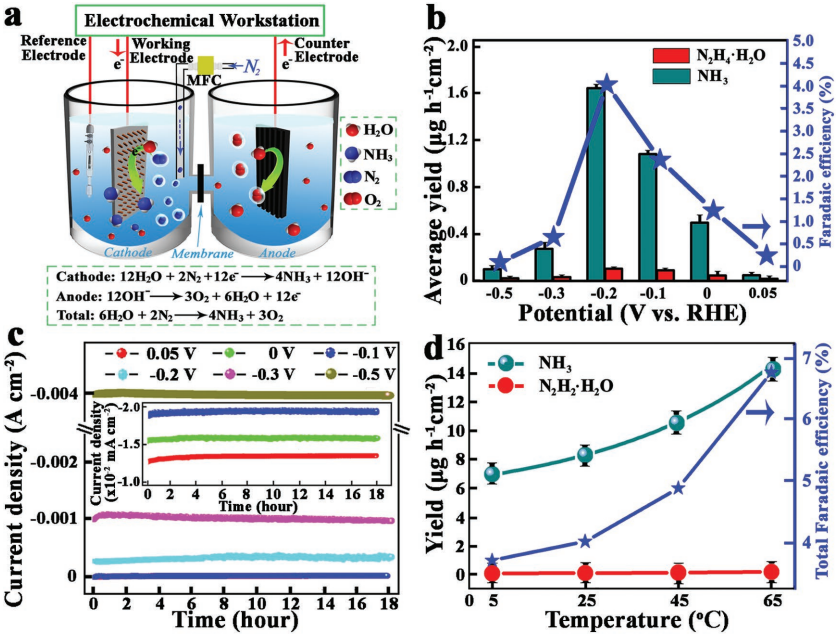

Figure 2. Electrocatalytic NRR on THH Au NRs. a) Schematic for electrocatalytic NRR (MFC is mass flow controller, membrane is Nafion 211 (Dupont)); b) Yield rate of ammonia (cyan), hydrazine hydrate (red) formation, and Faradic efficiency (blue) at each given potential; c) Chrono-amperometry results at the corresponding potentials; d) Yield of ammonia (cyan), hydrazine hydrate (red), and Faradic efficiency (blue) against catalytic temperature under atmospheric pressure at –0.2 V vs RHE; error bars in (b) and (d) represent the standard deviations of three independent measurements of the same sample.

using THH Au NRs as the cathodic catalysts, NRR is initiated at 0.05 V (vs RHE) with a measured Faradaic efficiency of 0.14% at room temperature and atmospheric pressure, which is slightly higher (≈0.048 V) than the anticipated standard potential. The remarkably enhanced activity is due to the abundant high-index facets (310) and (210) that are exposed on the catalyst, which provides a significant number of catalytically active sites to capture and dissociate N_2. Differing from previous reports,[23,24] both NH_3 and hydrazine hydrate ($N_2H_4 \cdot H_2O$) were detected after NRR for the first time, and the average yields and corresponding Faradaic efficiencies under various electrode potentials are listed in Table S3 (Supporting Information) (the calibration curves for colorimetric ammonia and hydrazine hydrate are shown in Figures S6–S8, Supporting Information). The NRR rate is shown in Figure 2b, the rate increases as the negative potential increases until –0.2 V vs RHE, where an average value of NH_3: 1.648 μg h^{-1} cm^{-2}, $N_2H_4 \cdot H_2O$: 0.102 μg h^{-1} cm^{-2} is measured. Beyond this negative potential, the reduction rate and Faradaic efficiency decrease significantly, which is attributed to the competitive adsorption of nitrogen and hydrogen species on the electrode surface. As the catalytic potential moves below –0.2 V vs RHE, the hydrogen evolution reaction becomes the primary process in this catalytic system, as demonstrated by the linear sweep voltammetric curve shown in Figure S9 (Supporting Information). Although the largest gap between Ar and N_2 is from –0.3 to –0.4 V, the highest yield of NRR is at –0.2 V vs RHE. As the electrochemical NRR is an equilibrium reaction competing with the H_2 evolution, the selection of optimum parameters for N_2 reduction requires an extreme sensitivity. Only under optimum conditions, the formation of NH_3 is preferred. As the working potential is –0.2 V vs RHE, the electrochemical NRR tends to occur. However, when the working potential is below –0.2 V vs RHE, the H_2 evolution would be the main reaction. It is reported that the electrolytic H atom will occupy catalytic sites of noble metals, which prohibits N_2 molecules adsorption on active sites.[25] For this reason, the NH_3 yield decrease and current density increase when the working potential ranges from –0.3 to –0.4 V. Additionally, to investigate the step surface catalytic effect of Au {730} on NH_3 synthesis, the comparison experiment using Au nanoparticles is conducted, and the scanning electron microscope (SEM) image is shown in Figure S10 (Supporting Information). After electrochemical NRR test, the N_2 reduction products are detected, with a NH_3 yield of 1.052 μg h^{-1} cm^{-2}, which is less than that of Au NRs, as shown in Figure S11 (Supporting Information).

For practical use, the durability of the catalyst for improved NRR is critical. To determine the durability, chronoamperometric tests were conducted. Figure 2c reveals that Au THH NRs demonstrate good NRR stability for the duration of 18 h. The recycling experiments have also been carried out, as shown in Figure S12a (Supporting Information), after 6th consecutive recycling, the catalyst ability exhibits a slight decline. Therefore, the obtained Au NRs after electrocatalytic N_2 reduction reaction were also sampled for HRTEM examination, as shown in Figure S12b (Supporting Information). It was found that the NRs were corroded and aggregated together during the catalytic process, which caused electrocatalytic activity to slightly decline after consecutive recycling.

By varying the N_2 flow rate, the N_2 reduction efficiency at room temperature and –0.2 V vs RHE was steady, without any apparent change, as shown in Figure S13 (Supporting Information). The approximate Faradic efficiency and yield of reduction products suggest that the rate of reduction is independent of the gas–solid interface and that N_2 is transported toward the cathodic catalysts' surface within the electrolyte. Additionally, the rate of the NRR is independent of the N_2 concentration in the liquid phase, which indicates that diffusion of N_2 is not the rate-determining step. By varying the performance temperatures of the NRR, the N_2 reduction efficiency at –0.2 V vs RHE can be determined, as shown in Figure 2d. In accordance with the Arrhenius equation, the reduction rate grows exponentially with the temperature, and the NRR yield is ≈2.1 times higher at 65 °C than at 5 °C. Under high temperature, the mass transfer rate of reactants is faster than low temperature conditions, as a result, mass transfer plays an important role in enhancing reaction rates in this work. Thermodynamic calculations show that the energy cost of ammonia synthesis via the industrial Haber–Bosch process is ≈335 kJ mol^{-1} in the absence of any catalysts.[26,27] However, the activation energy of N_2 reduction is only ≈13.704 kJ mol^{-1} when using the THH Au NRs according to the Arrhenius equation results, which significantly reduces the associated degree of difficulty; thus the NRR reaction can be conducted under mild conditions. To verify that the detected reduction products were generated via the NRR of Au NRs, four control experiments were performed: (i) An Ar gas flow is fed at –0.2 V (vs RHE) for 5 h; (ii) N_2 gas is introduced into the cell at open-circuit; (iii) Pristine carbon paper sheet and Nafion dispersed carbon sheet were used as working electrodes, respectively; (iv) Low concentrations of cetyltrimethyl ammonium bromide (CTAB) aqueous in electrolyte using pristine carbon paper sheet working electrode was tested. No reduction product is detected in either case, as shown in Figures S14–S17 (Supporting Information).

Based on the above analysis, a possible NRR process is depicted as follows: first, when N_2 and H_2O approach the surface of THH Au NRs, N_2 is weakly adsorbed on the Au stepped facets due to unsaturated coordination. Atoms at these locations serve as active sites for breaking and forming chemisorbed Au−N bonds, as shown in **Figure 3**. Second, due to the formation of steady N_2 reduction products, the activated H (produced from H_2O by electrolysis) spills over to form a more stable N−H bond and breaks the N≡N triple bond. Finally, hydrogenation of N_2 is carried out by adding H atoms one-by-one from the electrolyte and an electron from the electrode surface. To further determine the NRR mechanism, DFT was used to analyze the catalytic process; the features of the electronic structure and bonding states have also been established, and the geometry optimization is presented in Figure 3. The free-energy changes (ΔG, eV) of the partial elementary reactions are discussed in Table S4 (Supporting Information). As the free energy changes, the decreasing values of ΔG of reaction intermediates from NNH* to NHNH* and ΔG ($NHNH_2$* to NH_2NH_2) are greater than those of ΔG (NNH* to NNH_2*) and ΔG ($NHNH_2$ to NH*), respectively, as shown in Figure S18 (Supporting Information), and the NRR prefers to follow the alternating hydrogenation mechanism on THH Au NRs. This result differs from previous reports.[17,28] Furthermore, both

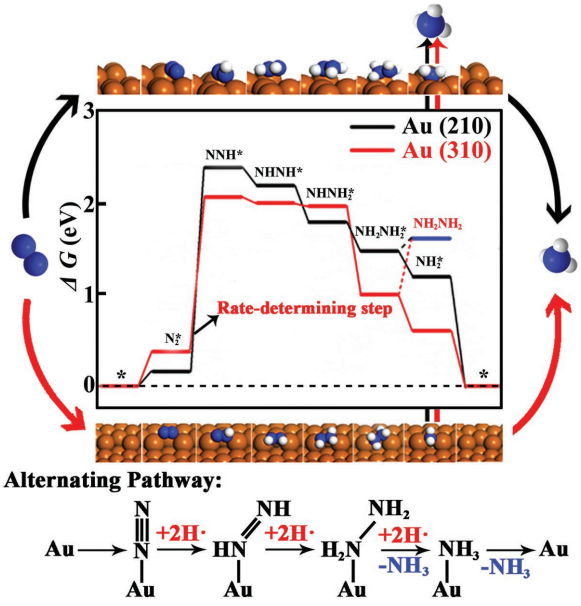

Figure 3. Free energy diagram and alternating hydriding pathway for NRR on Au (210) and Au (310) at equilibrium potential. For both Au (210) and Au (310), the rate-determining step is N_2 dissociation (reductive adsorption N_2* to form NNH*); after that, all the elementary reactions are exothermic except the formation of hydrazine hydrate from NH_2NH_2* intermediates.

NH_3 and $N_2H_4 \cdot H_2O$ are detected in our experiments, which further demonstrates the proposed alternate pathway.

In conclusion, to tackle the daunting challenges of artificially reducing N_2 under mild conditions, as a proof-of-concept experiment, we propose and demonstrate that the electrochemical reduction of N_2 to NH_3 at ambient conditions is indeed possible by using THH Au NRs as an electrocatalytic catalyst, even without the aid of activating complexes in the electrolyte. The reduction product yield rates are found to be as high as 1.648 and 0.102 μg h^{-1} cm^{-2} for NH_3 and $N_2H_4 \cdot H_2O$, respectively. Based on the DFT results and the fact that both NH_3 and $N_2H_4 \cdot H_2O$ are detected by colorimetric methods, an alternating hydrogenation mechanism can be safely carried out on THH Au NRs at room temperature and atmospheric pressure. Although the conventional Haber–Bosch process might remain the dominant method for ammonia production for some time, the proposed strategy and its promising electrochemical performance should spur interest toward using a more efficient catalyst for the electrochemical reduction of N_2. This process could also lead to a novel N_2/NH_3 cycle for storing and utilizing energy from different renewable sources, wherein N_2 and H_2O would be electrolytically transformed to NH_3 and O_2 in an electrolyzer powered by a renewable electricity source.

Experimental Section

Materials Preparation: The THH Au NRs were prepared using a seeded growth method. A binary surfactant mixture composed of CTAB and NaOL was utilized to improve the preparation. Details about the growth are described as follows: Briefly, the seed solution was made by fast injecting a freshly prepared ice-cold aqueous $NaBH_4$ solution (0.01 M, 0.6 mL) into an aqueous mixture of $HAuCl_4$ (0.01 M, 0.25 mL) and CTAB (0.1 M, 9.75 mL) under vigorous stirring. The resultant seed solution was kept at 30 °C for 30 min before use. To grow THH Au NRs, a growth solution was prepared, which was composed of CTAB (0.1 M, 40 mL), $HAuCl_4$ (0.01 M, 2.0 mL), and $AgNO_3$ (0.01 M, 0.1 mL). Under mild stirring, the solution became colorless gradually, after which the pH was adjusted to 1.9 with HCl (1.0 M, 0.8 mL). Ascorbic acid (0.1 M, 0.32 mL) was then added, and the solution was vigorously stirred for 30 s before 40 μL of the seed solution was injected in the growth solution, the mixture was stirred for another 30 s and left undisturbed overnight. The final products were washed several times by centrifugation (3000 rpm, 15 min) followed by removal of the supernatant and dispersion in water.

Calculation Method: First-principles calculations were performed using the DFT with the projector augmented wave pseudo potentials as implemented in the Vienna Ab initio Simulation Package.[29] The exchange-correlation functional was the generalized gradient approximation with the Perdew–Burke–Ernzerhof.[30] The cutoff energy for the plane wave-basis expansion was set to 500 eV and the atomic relaxation was continued until the forces acting on atoms were smaller than 0.01 eV $Å^{-1}$. The Brillouin zone was sampled with 5 × 5 × 1 Monkhorst–Pack k-point mesh, and the electronic states were smeared using the Fermi scheme with a broadening width of 0.1 eV. The van der Waals interaction was taken into account within DFT. The Au (210) and Au (310) surfaces observed in the experiment were modeled with 2 × 3 × 4 atom slabs separated by 15 Å of vacuum to avoid the unwanted interaction between the slab and its period images.

Calculation Details: Hydrogen atoms were added one by one to the adsorbed species, and DFT calculations were used to find the minimum energy configuration and vibrational frequencies. Several structures and adsorption sites were investigated in each case. All of the atoms were fully relaxed under geometry optimization. Frequencies of each complex were calculated after geometry optimization, and the free energy was obtained as follows: where $\triangle E$ is the total energy change, $\triangle E_{ZPE}$ and $\triangle S$ are the changes in zero-point energy and in entropy, respectively. T is the temperature (298.15 K), $\triangle G_U = -eU$, where U is the electrode potential with respect to the normal hydrogen electrode, and e is the transferred charge. $\triangle G_{pH} = k_B T \ln 10 \times pH$ where k_B is the Boltzmann constant, and pH = 13 for 0.1 M KOH electrolyte.

Supporting Information

Supporting Information is available from the Wiley Online Library or from the author.

Acknowledgements

This work was financially supported by Natural Science Foundation of China (Grants Nos. 51522101, 51471075, 51631004, and 51401084); Specialized Research Fund for the Doctoral Program of Higher Education of China (Grant No. 20110061120040); and General Financial Grant from the China Postdoctoral Science Foundation (Grant No. 2016M591498).

Note: The affiliations and affiliation order were updated on January 12, 2017, after initial publication online.

Received: September 6, 2016
Revised: September 24, 2016
Published online: November 11, 2016

[1] R. F. Service, *Science* **2014**, *345*, 610.
[2] V. Rosca, M. Duca, M. T. De Groot, M. T. M. Koper, *Chem. Rev.* **2009**, *109*, 2209.
[3] B. K. Burgess, D. J. Lowe, *Chem. Rev.* **1996**, *96*, 2983.
[4] S. Licht, B. C. Cui, B. H. Wang, F. F. Li, J. Lau, S. Z. Liu, *Science* **2014**, *345*, 637.

[5] M. A. H. J. Van Kessel, D. R. Speth, M. Albertsen, P. H. Nielsen, H. J. M. Op den Camp, B. Kartal, M. S. M. Jetten, S. Lucker, *Nature* **2015**, *528*, 555.
[6] U.S. Geological Survery, *Mineral Commodity Summaries 2016: U.S. Geological Survey*, U.S. Government Publishing Office, Washington, DC **2016**, p. 118.
[7] V. Smil, *Nature* **1999**, *400*, 415.
[8] K. Honkala, A. Hellman, I. N. Remediakis, A. Logadottir, A. Carlsson, S. Dahl, C. H. Christensen, J. K. Nørskov, *Science* **2005**, *307*, 555.
[9] P. J. Chirik, *Nat. Chem.* **2009**, *1*, 520.
[10] C. J. M. Van Der Ham, M. T. M. Koper, D. G. H. Hetterscheid, *Chem. Soc. Rev.* **2014**, *43*, 5183.
[11] V. Smil, *Enriching the Earth: Fritz Haber, Carl Bosch, and the Transformation of World Food Production*, MIT Press, Cambridge, MA **2004**.
[12] Y. M. Liu, S. Chen, X. Quan, H. T. Yu, *J. Am. Chem. Soc.* **2015**, *137*, 11631.
[13] F. L. Meng, H. X. Zhong, D. Bao, J. M. Yan, X. B. Zhang, *J. Am. Chem. Soc.* **2016**, *138*, 10226.
[14] H. X. Zhong, J. Wang, F. L. Meng, X. B. Zhang, *Angew. Chem. Int. Ed.* **2016**, *55*, 9937.
[15] C. Costentin, M. Robert, J. M. Saveant, *Chem. Soc. Rev.* **2013**, *42*, 2423.
[16] A. Hellman, E. J. Baerends, M. Biczysko, T. Bligaard, C. H. Christensen, D. C. Clary, S. Dahl, R. Van Harrevelt, K. Honkala, H. Jonsson, G. J. Kroes, M. Luppi, U. Manthe, J. K. Nørskov, R. A. Olsen, J. Rossmeisl, E. Skúlason, C. S. Tautermann, A. J. C. Varandas, J. K. Vincent, *J. Phys. Chem. B* **2006**, *110*, 17719.
[17] J. H. Montoya, C. Tsai, A. Vojvodic, J. K. Nørskov, *ChemSusChem* **2015**, *8*, 2180.
[18] Á. Logadóttir, J. K. Nørskov, *J. Catal.* **2003**, *220*, 273.
[19] Q. F. Zhang, L. L. Han, H. Jing, D. A. Blom, Y. Lin, H. L. Xin, H. Wang, *ACS Nano* **2016**, *10*, 2960.
[20] T. Ming, W. Feng, W. Q. Tang, F. Wang, L. D. Sun, J. F. Wang, C. H. Yan, *J. Am. Chem. Soc.* **2009**, *131*, 16350.
[21] Q. F. Zhang, Y. D. Zhou, E. Villarreal, Y. Lin, S. L. Zou, H. Wang, *Nano Lett.* **2015**, *15*, 4161.
[22] V. Kordali, G. Kyriacou, Ch. Lambrou, *Chem. Commun.* **2000**, 1673.
[23] A. Tsuneto, A. Kudo, T. Sakata, *J. Electroanal. Chem.* **1994**, *367*, 183.
[24] R. Lan, J. T. S. Irvine, S. W. Tao, *Sci. Rep.* **2013**, *3*, 1145.
[25] T. Oshikiri, K. Ueno, H. Misawa, *Angew. Chem. Int. Ed.* **2016**, *55*, 3942.
[26] N. D. Spencer, R. C. Schoonmaker, G. A. Somorjai, *J. Catal.* **1982**, *74*, 129.
[27] S. P. Stevenson, A. Sermon, *J. Chem. Soc., Faraday Trans.* **1987**, *83*, 2175.
[28] E. Skulason, T. Bligaard, S. Gudmundsdottir, F. Studt, J. Rossmeisl, F. Abild-Pedersen, T. Vegge, H. Jonssonac, J. K. Nørskov, *Phys. Chem. Chem. Phys.* **2012**, *14*, 1235.
[29] G. Kresse, J. Furthmüller, *Phys. Rev. B* **1996**, *54*, 11169.
[30] J. P. Perdew, K. Burke, M. Ernzerhof, *Phys. Rev. Lett.* **1996**, *77*, 3865.